JOURNAL OF SPACECRAFT AND ROCKETS
Vol. 43, No. 4, July–August 2006

Small Mission Design for Testing In-Orbit an Electrodynamic Tether Deorbiting System

P. Tortora*
University of Bologna, 47100 Forlì, Italy
L. Somenzi† and L. Iess‡
University of Rome "La Sapienza," 00184 Rome, Italy
and
R. Licata§
Alenia Spazio, 10146 Turin, Italy

The need to limit the population of artificial debris in near-Earth space motivates the development of efficient deorbiting propulsion systems. Electrodynamic tethers offer a valid and attractive alternative to conventional chemical thrusters because they impose a penalty in terms of deorbiting time rather than additional launch mass. A low-cost demonstration mission is designed, where a reduced-scale deorbiting system will be carried, deployed, and controlled by a microsatellite. Numerical simulations show that the proposed configuration of the electrodynamic system allows, even in absence of active tether current control, to maintain a stable tether attitude motion. This is obtained through a careful combination of bare and insulated tether segments. When active current control is applied, the tether libration angles are bounded to within 10 deg. The closed-loop control laws make use of the in-plane and out-of-plane libration angles and rates, which are estimated through a newly developed extended Kalman filter. The estimator's measurements are provided by two three-axis magnetometers mounted on the spacecraft structure and at the lower tether endpoint, respectively. It is shown that this microsystem is able to deorbit a low-Earth-orbit carrier spacecraft in about two months, demonstrating salient features of tether technologies and associated electrodynamic effects.

Nomenclature

A_t	=	tether cross section, πr_w^2
$\boldsymbol{b}$	=	magnetic field vector
C_{ED}	=	position of the center of application of the electrodynamic force
C_M	=	position of the tether system's center of mass
$\mathrm{d}\boldsymbol{x}$	=	differential element of the tether length
E_m	=	intensity of the induced electrical field along the tether
$\boldsymbol{F}_{\mathrm{ED}}$	=	total electrodynamic force acting on the tether
$I(x)$	=	current flowing into the wire
I_*	=	tether short-circuit current
i	=	nondimensional current flowing into the wire
i_s	=	orbital inclination
L	=	total length of the conductive segment of the tether
L_*	=	characteristic length typical of the bare tethers
L'	=	total length of the tether (conductive plus nonconductive segments)
l	=	nondimensional length of the conductive segment of the tether
M	=	total system's mass
m_b	=	mass of the ballast
m_c	=	mass of a single copper wire
m_k	=	mass of the Kevlar® tether
m_s	=	mass of the spacecraft
n_e	=	ionospheric plasma density
r_w	=	radius of the tether
$\boldsymbol{v}$	=	spacecraft orbital velocity
x	=	curvilinear coordinate on the tether with origin in the cathode
γ	=	mean deviation of the tether from the local vertical
δt	=	deorbiting time between two orbital altitudes
λ_D	=	Debye length of the Earth ionosphere
λ_k	=	Kevlar tether linear density
ξ	=	nondimensional curvilinear coordinate on the tether with origin in the cathode
σ_{al}	=	electrical conductivity of aluminum
σ_c	=	electrical conductivity of copper
$\boldsymbol{\tau}$	=	unity vector tangent to the tether
$\Phi(x)$	=	tether potential
ϕ	=	nondimensional tether potential

Received 1 January 2005; revision received 28 July 2005; accepted for publication 19 September 2005.

*Assistant Professor, II Facoltà di Ingegneria, Via Fontanelle 40; paolo.tortora@unibo.it. Member AIAA.

†Research Fellow, Dipartimento di Ingegneria Aerospaziale ed Astronautica, Via Eudossiana 18; somenzi@hermes.diaa.uniroma1.it.

‡Associate Professor, Dipartimento di Ingegneria Aerospaziale ed Astronautica, Via Eudossiana 18; iess@hermes.diaa.uniroma1.it. Member AIAA.

§Head, Robotic Systems, Corso Marche 41; rlicata@to.alespazio.it.

I. Introduction

A POTENTIALLY large demand for deorbiting propulsion systems is likely to grow in the near future, motivated by the need to limit the population of artificial debris in the near-Earth space. Because of the large mass penalty associated with the use of conventional chemical propellants, the development of more efficient, alternative systems is highly desirable. Electrodynamic (ED) tethers were proposed a few years ago[1,2] as a valid and attractive solution because they impose a penalty in terms of deorbiting time rather than additional launch mass. Moreover, the ability to operate with dead satellites can be envisaged, thus offering cost savings and capabilities unmatched by any other propulsion system. This feature is very attractive, especially to commercial users, who might otherwise be forced to deorbit a perfectly functioning satellite at the end of its nominal lifetime. On the contrary, disposal by means of ED tethers would allow maximizing the use of orbiting spacecraft (SC) until major internal failures occur. The original concept proposed in Refs. 1 and 2 was largely improved through the analysis carried out in Ref. 3, where the key role played by the contact impedances

associated with the coupling between the tether terminations and the ionospheric plasma was pointed out and precisely accounted for. In Ref. 4, an ED deorbiting system made up of an insulated tether, a passive inflatable collector at the positive termination, and a hollow cathode at the negative one was proposed; its deorbiting efficiency was assessed under realistic assumptions for its interaction with the ionospheric environment. This configuration formed the basis of a state-of-the-art ED tether system [ED orbital reentry device (EDOARD)] for deorbiting small- and medium-size low-Earth-orbit (LEO) satellites and launchers' upper stages, recently proposed[5,6] by an Italian team formed by Alenia Spazio and the University of Rome "La Sapienza."

Following these early studies, several ED tether deorbiting configurations were then analyzed in Refs. 7–10: In Ref. 7, the original ED deorbiting model proposed in Refs. 1 and 2 was improved to investigate and optimize the performance of the device, by developing a detailed numerical simulation that included models for tether dynamics, ED interactions with the Earth's ionosphere, and Spindt cathode electron emission. The software code used in Ref. 7 was then expanded in Ref. 8 to include the capability to model the deployment physics. A comparison of the deorbiting performance of several ED tethers, where the electron collection from the ionosphere is obtained with either simple bare wires or bare wires terminated with conducting spherical collectors, was carried out in Ref. 9. The comparative analysis, performed for the simple case of an equatorial orbit, shows that the use of the spherical collectors at the positive termination of the system significantly enhances the deorbiting capabilities of the electrodynamic bare tethers. The concept of ED drag applied to debris mitigation was also discussed in Ref. 10 where, in addition to a performance study of LEO and geostationary transfer orbit satellites ED deorbiting, the collision risk imposed by the selected deorbiting configuration was also analyzed and selected as the major parameter to be evaluated.

Among the ED tethers experimental activities already carried out in space,[11] it is worth mentioning the NASA Tethered Satellite System missions in 1992 (Ref. 12) and 1996 (Ref. 13), and the plasma motor generator system,[14] where, in a conductive tether attached to a Delta second stage, the current was driven in both directions, allowing both deorbiting and thrusting mode operations. In 1993–1994, the two Small Expendable Deployer System (SEDS) missions[15,16] took place to demonstrate the use of a close-loop control to deploy a 20-km-long tether. The Tether Physics and Survivability (TiPS) mission,[17] flown in 1996, was developed to study the long-term dynamics of a 4-km-long, nonconductive tether. Although TiPS was designed as a short-life (six-month), low-cost, secondary experiment, making use of essentially passive systems, it survived the orbital environment for many years, even after the laser ranging was discontinued in late 1997.

The Propulsive SEDS mission,[18] whose launch has been delayed many times and finally canceled in November of 2003, was intended for the ED deorbiting of a Delta stage, making use of a new concept of ED tether: The conductive wire was designed to be in direct contact with the ionospheric plasma (bare tether[19,20]), thus, collecting plasma electrons even without dedicated devices at the anodic endpoint.

The need to demonstrate and verify this type of ED tether-deorbiting technology and the associated space physics aspects has motivated the design of relatively small satellite missions[21] carrying different types of ED payloads and, more recently, a proposal for a microsatellite tether-deorbit experiment.[22]

With this aim, we have scaled down the original EDOARD[5,6] assembly to obtain a smaller and lighter system, and we have designed a low-cost demonstration mission, Micro-EDOARD, making use of a microsatellite as the carrier vehicle. In the proposed demonstration mission, the microsatellite will be provided by the University of Bologna [Alma Mater Satellite (ALMASat)].[23] Such a microsystem will still be able to demonstrate salient features of the tether technology and the ED effects on the space vehicle when orbiting in LEO.

The objectives of the proposed demonstration mission are related to ED tethers and are both technological and scientific. The technological objectives are associated with conductive tether and passive tether deployment mechanism design and tether dynamics and control. The main scientific objectives are identified with the in-orbit experimentation and validation of theoretical models of the well-known ED effect of the Earth's magnetic field crossed by a bare conductive tether.

The main contributions presented in this paper are threefold. First, we show that, because of an innovative tether deployer design, the ballast mass can be deployed passively with no need for a closed-loop control system, yielding a very simple, yet reliable, design. Second, we present a simplified analytical procedure to compute the center of application of the ED force along a bare tether. This procedure makes use of the hypothesis that, for tether currents sufficiently far from the short-circuit value, the voltage drop due to the electrical resistance of the tether itself can be neglected. Finally, we present a new estimator, based on the extended Kalman filtering methodology, whose state vector includes the tether in-plane and out-of-plane angles and rates. The sequential readings from two three-axis magnetometers (TAM) are used in the measurement vector and in the nonlinear observation function, respectively, to form the filter's measurement equation. This procedure renders the effective measurement noise nonstationary and state dependent, and this is addressed in the filter by computing an approximate time-varying noise covariance matrix.

The remainder of this paper is organized as follows: In the next section an overview of the mission is presented, along with a detailed description of the analytical method used for the optimization of the tether system configuration. This is followed by a numerical simulation of the tether passive deployment. The passive SC ED deorbiting is numerically simulated in Sec. III. This is followed by a description of the newly developed extended Kalman filter, where the tether angles and rates are estimated and its use in the closed-loop controlled deorbiting is described. A numerical simulation of an actively controlled SC deorbiting is then presented, showing that this strategy allows to bound the out-of-plane librations to very low values. Concluding remarks are offered in the last section.

II. Mission Profile and Tether System Configuration

The Micro-EDOARD experiment payload, comprising the tether, the tether deployer, ED subsystem, sensors, and mechanical, electrical, and data interfaces will be accommodated internally to the ALMASat SC. Current circulation in the tether is guaranteed by a hollow cathode, placed in the payload bay of the carrier SC, close to the spring mechanism shown in Fig. 1. This configuration has been selected to minimize the overall volume. Moreover, it is planned to accommodate a small wide-angle camera (not shown) on the deployment side of the microsatellite bus to monitor the full tether passive deployment operation during the proposed flight experiment.

Mission Timeline

In the proposed mission timeline, after the launch, a SC commissioning phase of about one month will begin, followed by about three months of continuous operations of the technological experiments carried onboard ALMASat. The deployment of the Micro-EDOARD payload will then occur, and the ED tether will be maintained fully operational (in its deorbiting electrical configuration) until the complete reentry of ALMASat. During the deorbiting phase, the SC altitude will be continuously tracked, making use of an onboard global positioning satellite receiver, until complete burning of the entire satellite bus in the Earth atmosphere.

The most promising launch opportunity we have identified is with the Russian–Ukrainian DNEPR launch vehicle (LV)[24] operated by the International Space Company (ISC) Kosmotras. This launcher is based on a converted intercontinental ballistic missile, the SS-18, and has already performed four successful cluster launches from the Baikonour cosmodrome located in Kazakhstan (in 1999, 2000, 2002, and 2004).

Until now, the DNEPR LV has launched only along medium-high inclination orbits. Informal contacts with the ISC Kosmotras are ongoing, to guarantee a DNEPR launch at lower inclinations, more suitable for the experimentation in orbit of an ED payload. However, because at the time being this dedicated launch has not

been confirmed yet, the analysis to be described has been carried out assuming that ALMASat carrying the Micro-EDOARD payload will be launched along the nominal 650-km altitude, 65-deg inclination DNEPR orbit.

As part of its research activity in the field of microsatellite design and manufacturing, the University of Bologna has installed a vhf–uhf amateur radio, fully automated ground station in the laboratories of the II Faculty of Engineering in Forlì, for communication with LEO satellites.[23] In its present configuration, it has been operational since September 2003, and L- and S-band communication facilities are scheduled to be installed in the next months. The Forlì ground station is proposed as the main ground support facility for the ALMASat mission carrying the Micro-EDOARD payload. Other stations (in particular the many amateur-radio ground stations installed by several universities all over the world) could be used in support of the proposed mission, to enhance the ground coverage and to give access to the ED telemetry data to a wide scientific community.

Tether System Configuration

The center of mass of an ED tethered system is usually very close to the SC center of mass because the latter represents the heaviest part of the system. If the dumbbell model is assumed for the tether, the center of application of the total Lorentz force acting on an insulated tether is placed a distance $L/2$ from the system's center of mass. (L is the total length of the conductive segment of the tether.) For a bare tether, it is shown later that this distance is comprised between $L/3$ and $L/2$. Thus, the ED force acts with a large arm, yielding a potentially large (destabilizing) torque, which, in turn, can give rise to a tumbling situation.

With the aim of designing an optimized tethered system where this intrinsic instability could be prevented, we have started our analysis from a basic configuration, where the SC (m_s) and the ballast (m_b) mass are 25 and 3.5 kg, respectively, and are connected by a bare copper wire of $L = 1$ km, with a radius $r_w = 0.3$ mm.

An analytical method aimed at the optimization of the ED tether configuration was presented in Ref. 25. This method allows the minimization of the Lorentz torque about the system's center of mass, by making use of properties of the bare tether current profile. The concept introduced in Ref. 25 is especially interesting in the dynamics of satellite orbit descent/raise, using ED tethers as thrusters. In Refs. 26 and 27, this design method was also extended to the case of ED tethers operating in the so-called generator (deboost) regime. The balance condition is obtained, in both cases, by properly adjusting the system's mass distribution. This is also the main limitation of the method because, in some cases, the mass distribution is an a priori design constraint determined by other mission requirements. This is the case for the ALMASat mission carrying the Micro-EDOARD payload. As a matter of fact, the mass of the carrier microsatellite has a lower bound determined by the SC bus and subsystems. Following the method presented in Refs. 25–27, a self-balanced ED tether could be obtained only by increasing the ballast mass (the deployer, in our case). This would impose serious penalties in terms of total system's mass because, following Ref. 27, the ballast mass would be increased from 3.5 to about 12 kg, thus, increasing the payload mass by about a factor of four.

Here we present a different approach, where the minimization of the Lorentz torque is obtained through the addition, on top the bare tether, of a nonconducting tether portion, typically with a negligible mass with respect to the whole system. A simplified analytical procedure to compute the length of this additional nonconductive tether segment is presented in the following paragraphs.

At the orbital altitude planned for the Micro-EDOARD demonstration mission $r_w \ll \lambda_D$, and then the charge collection of a bare tether obeys the orbital motion limit law. Let us introduce for convenience the following characteristic quantities:

$$L_* \simeq (\sigma_c/\sigma_{\rm al})^{\frac{2}{3}} (r_w/0.1\,{\rm mm})^{\frac{2}{3}} (E_m/100\,{\rm V/km})^{\frac{1}{3}} \times (10^{11}\,{\rm m}^{-3}/n_e)^{\frac{2}{5}} \cdot 2.66\,{\rm km}$$
$$I_* = \sigma_c E_m A_t \tag{1}$$

In Eqs. (1), $\sigma_c = 5.89 \times 10^7\ \Omega^{-1}{\rm m}^{-1}$ and $\sigma_{\rm al} = 3.5 \times 10^7\ \Omega^{-1}{\rm m}^{-1}$ are the electrical conductivity of copper and aluminum, respectively. When the nondimensional variables

$$\xi = x/L_*, \qquad i = I/I_*, \qquad \phi = \Phi/E_m L_*$$

are introduced, where $\Phi(x)$ is the voltage, the nondimensional current and potential profile along the tether can be written as[20]

$$\frac{{\rm d}i}{{\rm d}\xi} = -\frac{3}{4}\phi^{\frac{1}{2}}, \qquad \frac{{\rm d}\phi}{{\rm d}\xi} = 1 - i \tag{2}$$

The boundary conditions of Eqs. (2) are

$$i(l) = 0, \qquad \phi(0) = 0 \tag{3}$$

where $l = L/L_*$. The first condition is due to the lack of an electron collector balloon at the endpoint $\xi = l$, whereas the second is due to the presence of the hollow cathode, which almost grounds the cathodic termination to the ambient plasma.

A first-order approximation to the current profile along the tether can be computed by neglecting the voltage drop due to the electrical resistance of the tether itself, thus obtaining ${\rm d}\phi/{\rm d}\xi \simeq 1$ and, consequently, $\phi \simeq \xi$. It follows that

$$\left.\begin{aligned} &\frac{{\rm d}i}{{\rm d}\xi} \simeq -\frac{3}{4}\xi^{\frac{1}{2}} \\ &i(l) = 0 \end{aligned}\right\} \quad \Rightarrow \quad i(\xi) \simeq \frac{1}{2}\left(l^{\frac{3}{2}} - \xi^{\frac{3}{2}}\right) \tag{4}$$

The approximation in Eq. (4) is sufficient when the nondimensional current i is far from its short-circuit value ($i \ll 1$). Its validity can be verified a posteriori by computing the current in $\xi = 0$, to get $i(0) \simeq l^{3/2}/2$. The parameter l can be computed making use of

$$E_m \approx |\boldsymbol{v}||\boldsymbol{b}| \cos i_s \cos\gamma \tag{5}$$

If $\gamma \approx 0$ is assumed, then $E_m \approx 60$ V/km, which represents the mean value of the electric field acting on the system. Making use of Eq. (1), and supposing $n_e \approx 5 \times 10^{11}\ {\rm m}^{-3}$, we get $l = L/L_* \approx 0.2$, yielding $i(0) \approx 0.1 \ll 1$. For higher levels of n_e, which the system can experience during conditions of maximum solar illumination and at lower orbital altitudes, $i(0)$ can increase as much as $\approx$0.5, thus becoming nonnegligible with respect to the short-circuit value ($i = 1$). However, these conditions are reached only during the final stage of the deorbiting phase, so that the approximation in Eq. (4) is valid most of the time.

With these assumptions, the mean current along the tether can be computed by

$$I_m = \frac{1}{L}\int_0^L I(x)\,{\rm d}x = \frac{I_*}{l}\int_0^l i(\xi)\,{\rm d}\xi = \frac{3}{10} l^{\frac{3}{2}} I_* \approx 65\,{\rm mA} \tag{6}$$

and the total ED force acting on the tether is given by

$$\boldsymbol{F}_{\rm ED} = \int_0^L I(x)\,{\rm d}\boldsymbol{x} \times \boldsymbol{b} \tag{7}$$

where ${\rm d}\boldsymbol{x}$ is the differential element of the tether length. Given the low current levels, $\boldsymbol{F}_{\rm ED}$ is also small, so that the deviations of the tether from the dumbbell model (assumed at the beginning of this section) can be neglected. Hence, define $\boldsymbol{\tau}$ as a unity vector tangent to the tether, then ${\rm d}\boldsymbol{x} = {\rm d}x\,\boldsymbol{\tau}$ and the ED force becomes

$$\boldsymbol{F}_{\rm ED} = (\boldsymbol{\tau} \times \boldsymbol{b}) \int_0^L I(x)\,{\rm d}x = I_m L(\boldsymbol{\tau} \times \boldsymbol{b}) = I_m \boldsymbol{L} \times \boldsymbol{b} \tag{8}$$

where $\boldsymbol{L} = L\boldsymbol{\tau}$. For $I_m \approx 65$ mA, force $F_{\rm ED} \triangleq |\boldsymbol{F}_{\rm ED}| \approx 0.85$ mN.

To quantify the ED-induced torque, we now have to analyze the relative position of the center of mass C_M and the center of application of the ED force, $C_{\rm ED}$. We have

$$C_{\rm ED} = \frac{1}{F_{\rm ED}}\int_0^L x I(x) |{\rm d}\boldsymbol{x} \times \boldsymbol{b}| \tag{9}$$

and making use of Eqs. (4–8),

$$C_{\mathrm{ED}} = \frac{1}{I_m L}\int_0^L I(x)x\,\mathrm{d}x = \frac{5}{14}L \tag{10}$$

This value is slightly underestimated because the voltage drop toward the cathode has been neglected. The position of the center of mass, computed in a reference frame centered on the SC (cathode) is

$$C_M = (L/M)(m_b + m_c/2) \tag{11}$$

where M is the total system's mass and $m_c = 2.5$ kg is the mass of the copper wire. With the basic configuration as earlier selected, $C_M \approx 3/20L$. The arm of the ED torque is then $C_{\mathrm{ED}} - C_M \approx L/5 = 0.2$ km, a value large enough to induce tumbling in the tethered satellite system.[28–30]

An optimization procedure can be performed to minimize the distance between C_{ED} and C_M. First, when the SC deorbiting time is considered, the approximate expression given in Ref. 3 relating the deorbiting time δt between two orbital altitudes can be used:

$$\delta t_{a_1 \to a_2} \approx \left(5 \times 10^{-10} \Big/ \cos i_s\right)(M/LI)a^{\frac{5}{2}}\Big|_{a_1}^{a_2} \tag{12}$$

which yields a δt of about four months when the design data of the basic configuration are used: $I = 65$ mA, $a_1 = (6378 + 650) \times 10^3$ m, $a_2 = (6378 + 200) \times 10^3$ m, and $i_s = 65$ deg. Thus, it is shown that, to obtain the target deorbiting time of two months, the tether current must be almost doubled, which can be easily obtained by keeping constant the length of the bare tether segment, but making it a double-strand tether. Moreover, this choice allows the minimization of the risk due to a destructive orbital debris impact[31,32] and to obtain a fail-safe tether configuration[33,34] without changing the position of C_{ED}.

The easiest way to reduce the distance between C_{ED} and C_M is a change in the position of C_M, which can be obtained by adding an insulated wire segment at the top end (toward the anode) of the bare tether. We have selected the nonconducting Kevlar®-49 wire, for its light weight characteristics, with density of 1.45 g/cm^3, and excellent mechanical properties. To compute the new optimal total length of the tether L' (copper and Kevlar), we write

$$\begin{aligned} C_M &= (1/M)\left[m_b L' + m_c L + (\lambda_k/2)(L'^2 - L^2)\right] \\ &= (1/M)[m_b L' + m_c L + (m_k/2)(L' + L)] \end{aligned} \tag{13}$$

where λ_k and m_k are the Kevlar linear density ($\lambda_k \approx 0.4$ kg/km, for a $r_w = 0.3$ mm) and mass, respectively. We can use Eqs. (10) and (13) to write

$$C_M = C_{\mathrm{ED}} \Rightarrow (1/M)\left[m_b L' + m_c L + (\lambda_k/2)(L'^2 - L^2)\right] = (5/14)L \tag{14}$$

The solution to Eq. (14) can be found by defining $M \triangleq m_s + 2m_c + m_b + \lambda_k(L' - L)$ and $M' \triangleq m_s + 2m_c + m_b$, so that $M = M' + \lambda_k(L' - L)$. Substituting in Eq. (14), one gets:

$$\begin{aligned} &(\lambda_k/2)L'^2 + [m_b - (5/14)\lambda_k L]L' \\ &\quad + L[-(5/14)M' + m_c - (\lambda_k/7)L] = 0 \end{aligned} \tag{14'}$$

which is a second-degree equation in the total tether length L'. Solving Eq. (14′) and making use of the values $m_s = 25$ kg, $m_b = 3.5$ kg, $\lambda_k = 0.4$ kg/km, $m_c = 2.5$ kg, and $L = 1$ km, as described earlier, one gets a negative (meaningless) and a positive solution yielding $L' \cong 2.4$ km. Indeed, numerical simulations reported later show that a system with a 1-km double-strand copper wire weighing 5 kg and a 1.4-km single Kevlar wire weighing 0.56 kg possesses the target stability and deorbiting properties. Such a system is hereinafter considered the optimized configuration to be used in the numerical simulations of both the passive deployment and the deorbiting phase.

III. Passive Tether Deployment

A key point for an efficient ED deorbiting system is the tether deployment dynamics. A comprehensive study was performed in Refs. 35 and 36, through an asymptotic analysis for small values of the nondimensional parameter ε, directly proportional to the linear density of the tether, to the square of the ejection velocity and inversely proportional to the characteristic value of the tension of the tether. It has been shown that, to obtain a deployment scheme with zero final libration, a two-stage process is necessary where the tether tension is indirectly controlled to get, first, a constant radial velocity of the end mass and, then, an exponential deployment. This is obtained through an accurate control of the reel's unwinding angular velocity.

To minimize mass, volume, and complexity, however, the design of Micro-EDOARD adopts a passive tether deployment strategy, initiated by an impulsive actuation imparted by a spring separation mechanism and commanded from ground. This impulse (yielding the initial relative velocity between the ballast mass and the carrier spacecraft) must be sufficient to allow the deployment of enough tether for gravity gradient effects to take over and guarantee the remainder of deployment. Because, in the early phase of the deployment, the acting dynamic forces are rather small, to guarantee the successful completion of a passive deployment, the tether unwinding friction forces must be kept very small. For this purpose, a large amount of work has been performed in the Turin plant of Alenia Spazio, where a Tether Mechanism Materials and Manufacture Program was established under ESA contracts.[37] Among the other remarkable results achieved by that program, an interesting outcome is the evaluation of the friction forces exerted by the spool on the unwinding tether, under different deployment rate and angle conditions and using spools with different geometrical properties. It turned out that the friction follows, in most cases, a law proportional to the deployment rate.[38] This is certainly true for deployment rates larger than 1 m/s, the lower limit for the experimental test setup assembled at Alenia Spazio. For deployment rates smaller than 1 m/s, the particular design of the Micro-EDOARD deployer allows to extrapolate these results down to zero velocity. This assumption, although not completely provable, can be considered acceptable when deployment rates close to zero occur when a certain portion of the tether has been already deployed. In this case, the gravity gradient force is large enough to restart the deployment even if the deployment friction is not exactly zero.

In the case of the Micro-EDOARD tether system, where a relatively short tether has to be deployed, the spool will be deployed together with the tether, constituting the ballast mass at the end of the deployment itself (Fig. 1). This means that there is no way to control the deployment rate actively through an electric motor. The deployment rate is essentially driven by the external forces (gravity gradient and Coriolis) and by the spool friction.

A computer simulation has been carried out to verify that, given a range of initial relative velocities between the SC and the spool (ballast mass), the deployment could take place correctly and that the final deployment rate does not exceed a fixed limit, for example, 0.5 m/s. The equations of motion have been numerically integrated, using a standard fourth-order Runge–Kutta (RK) algorithm, in a rotating orbital reference frame, with origin in the center of mass of the system. The orbital reference frame is defined as ($\boldsymbol{r}$, $\boldsymbol{\vartheta}$, $\boldsymbol{h}$), where $\boldsymbol{r}$ is the unity vector directed from the center of the Earth to center of mass of the tether system, $\boldsymbol{h}$ is in the direction of the orbit normal, and $\boldsymbol{\vartheta}$ completes a right-handed reference frame. (It is in the direction of the SC velocity, for circular orbits.) The mathematical model for the differential equations integrated through the RK integrator has been derived applying the equilibrium of forces acting on the S/C and ballast mass, respectively. Each of those masses is subjected to a gravity gradient force directed along the orbital axis $\boldsymbol{r}$, whose absolute value can be approximated as $3mx\omega_0^2$ (Ref. 11), where m is the SC or the ballast mass, x is the distance between the mass m and the system's center of mass, and ω_0 is the system's orbital mean motion. Moreover, the Coriolis force $-2m\boldsymbol{\omega}_0 \times \boldsymbol{v}$ is acting on each of the two masses m, where $\omega_0 = [0 \;\; 0 \;\; \omega_0]$ and $\boldsymbol{v}$ are the orbital mean motion vector and the velocity vector of the mass

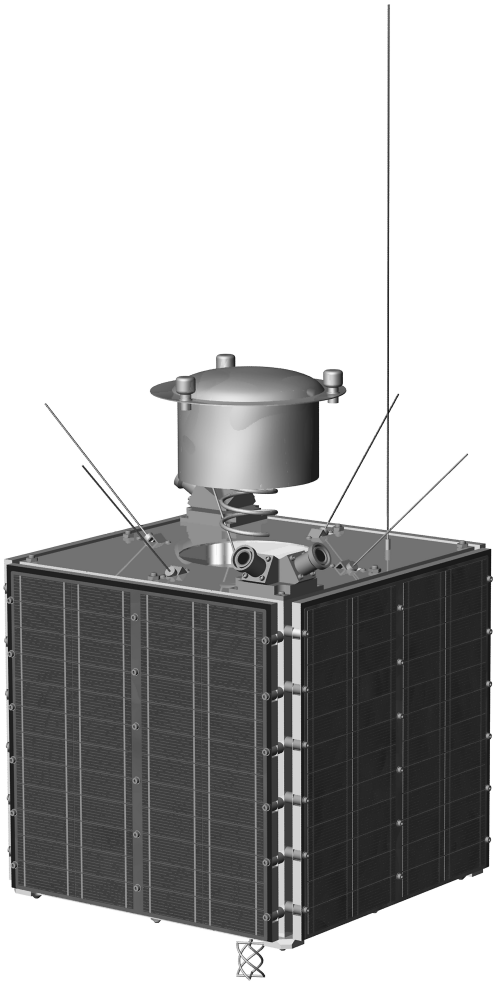

Fig. 1 ALMASat spacecraft, carrying the micro-EDOARD payload.

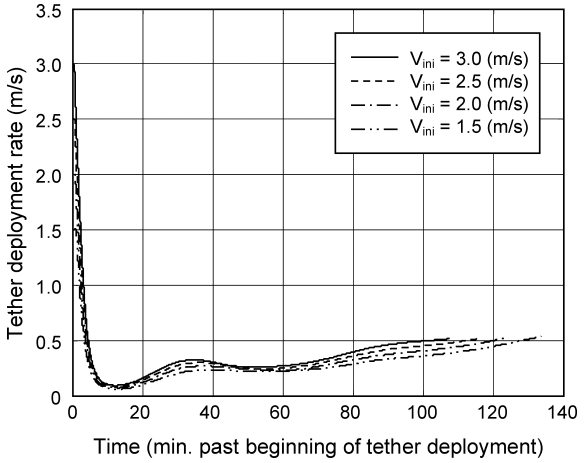

Fig. 2 Tether length vs time for different initial deployment rates.

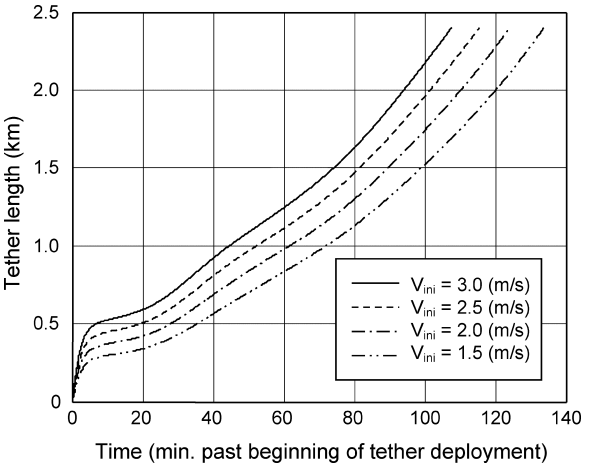

Fig. 3 Tether deployment rate vs time for different initial deployment rates.

m in the orbital reference frame, respectively. During deployment, the tether system also experiences the drag due to the friction of the tether on the deployer. Even if originated only at the deployer end point, this friction reflects in an increased tether tension, which, in turn, originates a force on the two masses, opposite to the deployment direction. For the first tether segment, this force is assumed to vanish, because of the particular tether deployer design, where the first 100 m of copper wire are wound around the external part of the spool (Fig. 1). According to the results presented in Ref. 38, when the tether length is larger than 0.1 km, this force (equally applied at both end masses) is assumed proportional to the deployment rate:

$$f = 0, \qquad 0 \le d_t \le 0.1\,\text{km}$$
$$f = 0.05\,\text{kg/s} \cdot v, \qquad 0.1 \le d_t \le 2.4\,\text{km} \tag{15}$$

where d_t is the deployed tether length and v is the deployment rate (the time derivative of d_t).

With the mathematical model just described, we have simulated the deployment of the ballast mass from the carrier SC for initial relative velocities in the range [1.5, 3] m/s. The simulated SC orbit is a circular one with an altitude of 300 km, and the deployment is initiated with a direction parallel to the orbital $\boldsymbol{r}$ axis. The numerical results show that when the friction starts acting on the tether, a sudden velocity reduction is experienced during the deployment (Fig. 2); it almost nullifies the initial relative velocity, so that the final velocity becomes almost independent of the initial conditions. The only appreciable difference is the total deployment time (Fig. 3), which ranges from about 105 to about 135 min for the fastest and slowest deployments, respectively.

IV. Passive Deorbiting Performance

With the optimized tether configuration obtained in Sec. II, we have numerically simulated the complete deorbiting of the SC ALMASat, carrying the Micro-EDOARD payload. We used a dumbbell tether and modeled the environmental ionosphere and geomagnetic field according to the International Reference Ionosphere and a 10th-order International Geomagnetic Reference Field (IGRF) model, respectively. The solar activity, which is an input to the simulations, was set at a constant average value equal to 150 flux units at 10.7 cm, during the whole deorbiting phase. The aerodynamic forces were not included in the numerical code because it is verified that their additional drag has the effect of shortening the deorbiting time of the SC. Moreover, the resulting aerodynamic torque, counterbalanced by the gravitational torque, slightly deviates the attitude of the tether from the local vertical. The tether's attitude was initialized with zero libration angles and rates.

Starting from its nominal altitude of 650 km and flying along a circular orbit with an inclination of 65 deg, the ED tethered system is deorbited in about two months (solid line in Fig. 4), with an increasing orbital decay rate at lower altitudes due to the augmented current flowing into the tether. Following Ref. 4, we can say that the deorbiting time increases by about 43% when the level of the solar activity is minimum (78 flux units at 10.7 cm), whereas it diminishes by about 20% when this level reaches maximum values (200 flux units at 10.7 cm). In our simulations, the tether current is left completely uncontrolled, as is the tether attitude, thus being driven only by the varying environmental conditions (ionospheric plasma density and local magnetic field) and tether libration angles. On the other hand, the tether attitude is dominated by the current itself, which pumps energy into the system,[28–30] through the external

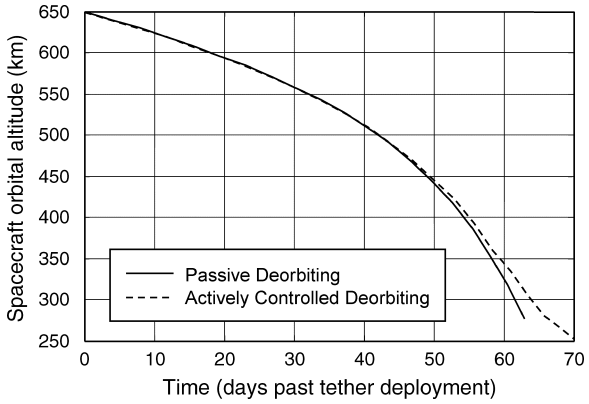

Fig. 4 ALMASat orbital altitude vs deorbiting time.

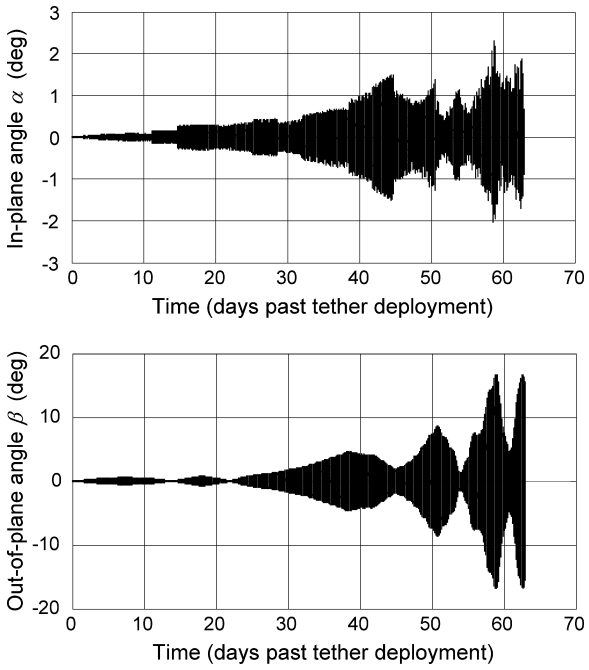

Fig. 5 Tether libration angles vs deorbiting time, uncontrolled attitude.

ED torque M_{ED}, subsequently described in Eq. (29). As shown in Fig. 5, the in-plane α and out-of-plane β libration angles are automatically bounded to within 2.5 and 20 deg, respectively. This has been obtained through the described optimization of the lengths of the bare and nonconductive tether segments, yielding an almost vanishing arm of the ED force. Moreover, for the first 50 days, the libration angles are bounded to even lower values, thus, confirming the excellent agreement of the approximate model presented in Sec. II with the numerically simulated system. When the current intensity exceeds the values for which the voltage drop along the tether is no longer negligible, the distance between C_{ED} and C_M increases, so that the ED torque causes an evident amplification of the libration angles (especially the out-of-plane motion).

V. Closed-Loop Control of Tether Deorbiting

An actively controlled deorbiting is attractive because it offers both the possibility to vary the orbital decay rate and to control to within specific values the tether libration angles. An efficient method to control the tether attitude was presented in Ref. 39 based on the knowledge of the in-plane and out-of plane libration angles and rates, α, β, $\dot{\alpha}$, and $\dot{\beta}$, and the magnetic field vector in the orbital reference frame. This method requires the evaluation of a nondimensional Lyapunov function and the total ED power and switches the tether current off when both exceed certain thresholds. Because this control method is applied in the context of the proposed mission, the main equations are recalled in the following paragraphs.

The Lyapunov function is computed starting from Euler's rigid-body equations of motion, where the ED torque is neglected, which are then multiplied by the body angular velocity relative to the rotating orbital frame. Integration of these equation yields the Hamiltonian of the system (see Ref. 39)

$$H = \tfrac{1}{2}\boldsymbol{\omega}_{\mathrm{rel}} \cdot \boldsymbol{J}\boldsymbol{\omega}_{\mathrm{rel}} + \tfrac{3}{2}J\omega_0^2 \boldsymbol{r} \cdot \boldsymbol{J}\boldsymbol{r} - \tfrac{1}{2}\omega_0^2 \boldsymbol{h} \cdot \boldsymbol{J}\boldsymbol{h} = \text{const} \tag{16}$$

the three terms involved being the kinetic energy, gravity gradient, and centrifugal potential, respectively. In Eq. (16), $\boldsymbol{J} = \mathrm{diag}\{0 \;\; J \;\; J\}$ and J is the tether moment of inertia along the body axes $\boldsymbol{j}$ and $\boldsymbol{k}$ (whereas it vanishes along the $\boldsymbol{i}$ axis). For the equilibrium configuration, $\alpha = \beta = \dot{\alpha} = \dot{\beta} = 0$ so that

$$H_0 = -\tfrac{1}{2}J\omega_0^2 \tag{17}$$

The selected Lyapunov function is then

$$V = H - H_0 = \tfrac{1}{2}\boldsymbol{\omega}_{\mathrm{rel}} \cdot \boldsymbol{J}\boldsymbol{\omega}_{\mathrm{rel}} + \tfrac{3}{2}J\omega_0^2 \boldsymbol{r} \cdot \boldsymbol{J}\boldsymbol{r} + \tfrac{1}{2}J\omega_0^2 - \tfrac{1}{2}\omega_0^2 \boldsymbol{h} \cdot \boldsymbol{J}\boldsymbol{h} = \text{const} \tag{18}$$

Observing that $V = \text{const}$ and that $\dot{V} = 0$, the Lyapunov theorem ensures simple but not asymptotic stability. Equation (18) can be written in nondimensional form:

$$\tilde{V} = V/|H_0| = 2V \Big/ J\omega_0^2 \tag{18'}$$

and expressing it in terms of libration angles and rates, one gets

$$\tilde{V} = \left(1 \Big/ \omega_0^2\right)(\dot{\beta}^2 + \dot{\alpha}\cos^2\beta) + 3\sin^2\alpha + 3\cos^2\alpha\sin^2\beta + \sin^2\beta \tag{18''}$$

Computation of the Lyapunov function for a tether lying in the $(\boldsymbol{\vartheta}, \boldsymbol{h})$ plane of the orbital reference frame, with $\boldsymbol{\omega}_{\mathrm{rel}} = 0$ (where $\alpha = \pi/2$, $\beta = \bar{\beta}$, and $\dot{\alpha} = \dot{\beta} = 0$, with $\bar{\beta}$ any value between 0 and 2π) yields $\tilde{V} = 3 + \sin^2\bar{\beta}$, which clearly has a minimum for $\bar{\beta} = 0$. The value $\tilde{V} = 3$ defines the energy limit above which tumbling may occur. If the ED tether circuit is opened when $\tilde{V}$ reaches this value, the tether cannot flip over. Of course, safe operations require setting the energy threshold to a somewhat lower level.

Thus, the stability condition based on the Lyapunov function defines the energy bound for systems under the effect of gravity gradient torque. Unfortunately, extension of this method to the case where (variable) magnetic torques are acting on the tether is very complex. The monitoring of the Lyapunov function in Eq. (18″) and the activation of a control law when the ED torque causes $\tilde{V}$ to exceed the selected threshold are much easier. The simplest implementation of a control law phases the current flaw in the tether so that the ED torque actually reduces the system's energy. This can be easily obtained by controlling only the sign of the mechanical power $\boldsymbol{M}_{\mathrm{ED}}\,\boldsymbol{\omega}$. When the power is negative, the ED torque is subtracting energy from the attitude motion and the current may flow in the wire, producing orbital decay. When the sign is positive, the circuit must be opened to avoid further energy pumping.

For the control laws presented in Ref. 39 to be applied to the Micro-EDOARD mission, we must, therefore, be able to estimate onboard, and in realtime, the four variables α, β, $\dot{\alpha}$, and $\dot{\beta}$. Previous studies[40,41] were carried out for one of the earliest space tether experiments in space[15] showing that the libration angles and rates (and other interesting variables governing the tether dynamics) could be accurately estimated in real time, either making use of several distributed sensors, or adding a direct out-of-plane libration angle measurement device. As it is shown in the following paragraph, however, the same goal can be accomplished efficiently using two low-cost sensors, yet obtaining very accurate results.

Extended Kalman Filter Design

The proposed estimator consists of a self-initializing extended Kalman filter (EKF). The filter's state vector $\boldsymbol{x} = [\alpha \;\; \beta \;\; \dot{\alpha} \;\; \dot{\beta}]^T$ consists of the in-plane and out-of-plane tether angles and rates with respect to the orbital reference frame defined earlier.

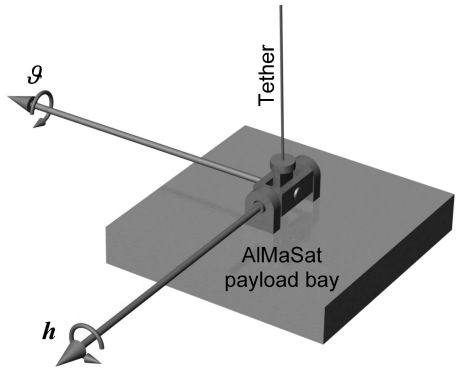

Fig. 6 Two-axis joint at the tether lower endpoint.

Measurement Model

It is assumed that the SC has two TAMs onboard. One is mounted inside the bus, and the other is at the lower tether endpoint. The latter is fixed to a two-axis joint, which allows only rotations about the $\boldsymbol{h}$ axis (α angles) and about the ϑ axis (β angles), as shown in Fig. 6.

If $\boldsymbol{b}^{\text{sat}}$ is the magnetic field vector in the SC body axes and $\boldsymbol{b}^{\text{tet}}$ is the magnetic field vector in the tether reference frame, they are related by the following equation:

$$\boldsymbol{b}^{\text{tet}} = \boldsymbol{R}^{\text{TS}}\boldsymbol{b}^{\text{sat}} \tag{19}$$

where $\boldsymbol{R}^{\text{TS}}$ is the rotation matrix between the SC body axes and the tether reference frame. If the SC is three-axis stabilized, and the attitude is controlled in the so-called Earth-pointing mode, the $\boldsymbol{R}^{\text{TS}}$ matrix is defined as

$$\boldsymbol{R}^{\text{TS}} = \begin{bmatrix} c_\alpha c_\beta & s_\alpha c_\beta & -s_\beta \\ -s_\alpha & c_\alpha & 0 \\ c_\alpha s_\beta & s_\alpha s_\beta & c_\beta \end{bmatrix} \tag{20}$$

where c_x and s_x indicate $\cos(x)$ and $\sin(x)$, respectively.

The TAMs readings at time t_k are related to the true magnetic field via

$$\tilde{\boldsymbol{b}}_k^{\text{tet}} = \boldsymbol{b}_k^{\text{tet}} + \boldsymbol{v}_k^{\text{tet}} \tag{21}$$

$$\tilde{\boldsymbol{b}}_k^{\text{sat}} = \boldsymbol{b}_k^{\text{sat}} + \boldsymbol{v}_k^{\text{sat}} \tag{22}$$

where it is assumed that the stationary measurement noise has the same statistical properties for both TAMs and is distributed as

$$\boldsymbol{v}_k^{\text{sat}} \equiv \boldsymbol{v}_k^{\text{tet}} \sim N(0, \boldsymbol{R}_{\text{TAM}}) \tag{23}$$

and the covariance $\boldsymbol{R}_{\text{TAM}}$ is known. Moreover, the cross correlation between the two TAMs measurement noise is, namely, zero so that

$$E\left[\left(\boldsymbol{v}_k^{\text{sat}}\right)\left(\boldsymbol{v}_k^{\text{tet}}\right)^T\right] = E\left[\left(\boldsymbol{v}_k^{\text{tet}}\right)\left(\boldsymbol{v}_k^{\text{sat}}\right)^T\right] = 0 \tag{24}$$

where E is the mathematical expectation.

To derive the nonlinear filter's measurement equation based on Eq. (19), we can set $\boldsymbol{z}_k = \tilde{\boldsymbol{b}}_k^{\text{tet}}$ and $\boldsymbol{h}_k = \boldsymbol{R}_k^{\text{TS}}\tilde{\boldsymbol{b}}_k^{\text{sat}}$ to obtain

$$\boldsymbol{z}_k = \boldsymbol{h}_k\left(\alpha, \beta, \tilde{\boldsymbol{b}}_k^{\text{sat}}\right) + \boldsymbol{n}_k \tag{25}$$

where $\boldsymbol{n}_k$ is the effective measurement noise defined as

$$\boldsymbol{n}_k = \boldsymbol{v}_k^{\text{tet}} - \boldsymbol{R}_k^{\text{TS}}\boldsymbol{v}_k^{\text{sat}} \tag{26}$$

Note that this noise is nonstationary and state dependent (through the matrix $\boldsymbol{R}_k^{\text{TS}}$). The state dependency of the measurement noise is handled in an approximate manner, according to the usual practice in attitude estimation EKF algorithms, by substituting the estimated values of the state for the true values at each time instant. The covariance of the effective measurement noise $\boldsymbol{n}_k$ is

$$\begin{aligned} \boldsymbol{R}_k^n &= E\left[\boldsymbol{n}_k\boldsymbol{n}_k^T\right] = E\left[\left(\boldsymbol{v}_k^{\text{tet}} - \boldsymbol{R}_k^{\text{TS}}\boldsymbol{v}_k^{\text{sat}}\right)\left(\boldsymbol{v}_k^{\text{tet}} - \boldsymbol{R}_k^{\text{TS}}\boldsymbol{v}_k^{\text{sat}}\right)^T\right] \\ &= E\left[\left(\boldsymbol{v}_k^{\text{tet}}\right)\left(\boldsymbol{v}_k^{\text{tet}}\right)^T\right] - E\left[\left(\boldsymbol{v}_k^{\text{tet}}\right)\left(\boldsymbol{v}_k^{\text{sat}}\right)^T\left(\boldsymbol{R}_k^{\text{TS}}\right)^T\right] \\ &\quad - E\left[\boldsymbol{R}_k^{\text{TS}}\left(\boldsymbol{v}_k^{\text{sat}}\right)\left(\boldsymbol{v}_k^{\text{tet}}\right)^T\right] + E\left[\boldsymbol{R}_k^{\text{TS}}\left(\boldsymbol{v}_k^{\text{sat}}\right)\left(\boldsymbol{v}_k^{\text{sat}}\right)^T\left(\boldsymbol{R}_k^{\text{TS}}\right)^T\right] \\ &= \boldsymbol{R}_{\text{TAM}} + \left(\boldsymbol{R}_k^{\text{TS}}\right)\boldsymbol{R}_{\text{TAM}}\left(\boldsymbol{R}_k^{\text{TS}}\right)^T \cong 2\boldsymbol{R}_{\text{TAM}} \end{aligned} \tag{27}$$

The last equality in Eq. (27) holds exactly if the "true" $\boldsymbol{R}_k^{\text{TS}}$ is used in the filter. Because, of course, only the estimated $\boldsymbol{R}_k^{\text{TS}}$ is available, this is used for the real-time computation of the effective measurement noise covariance matrix $\boldsymbol{R}_k^n$. Note the setting $\boldsymbol{R}_k^n \cong 2\boldsymbol{R}_{\text{TAM}}$ avoids any correlation between the measurement and the process noise.

The observation matrix $\boldsymbol{H}_k$, needed for the calculation of the Kalman gains, is computed as $\boldsymbol{H}_k = \partial\boldsymbol{h}/\partial\boldsymbol{x}|_{x=\hat{x}}$.

State Propagation

Euler's equations representing the attitude dynamics of the tether (using the dumbbell model) are given by

$$\begin{aligned} \ddot{\alpha} - 2(\dot{\alpha} + \omega_0)\dot{\beta}\tan\beta &= [(\boldsymbol{M}_G + \boldsymbol{M}_{\text{ED}}) \cdot \boldsymbol{k}]/J\cos\beta \\ \ddot{\beta} + (\dot{\alpha} + \omega_0)^2\sin\beta\cos\beta &= -[(\boldsymbol{M}_G + \boldsymbol{M}_{\text{ED}}) \cdot \boldsymbol{j}]/J \end{aligned} \tag{28}$$

where $\boldsymbol{M}_G$ and $\boldsymbol{M}_{\text{ED}}$ are the gravitational and ED torques, respectively. The explicit expressions of the mentioned torques are given by

$$\boldsymbol{M}_G = 3(\mu/a^3)\boldsymbol{r} \times \boldsymbol{J}\boldsymbol{r} \tag{29}$$

$$\boldsymbol{M}_{\text{ED}} = d_{\text{ED}}\boldsymbol{\tau} \times \boldsymbol{F}_{\text{ED}} = d_{\text{ED}}I_m L\boldsymbol{\tau} \times (\boldsymbol{\tau} \times \boldsymbol{b}) \tag{30}$$

where μ is the Earth gravitational parameter, a is the distance between the Earth center of mass and the system's center of mass, and d_{ED} is the distance between C_M and C_{ED}.

Let $\dot{x}_1 = x_3$ and $\dot{x}_2 = x_4$, so that Eqs. (28) become

$$\begin{aligned} \dot{x}_3 &= 2(x_3 + \omega)x_4 t_{x_2} + \left[-3J\omega^2 s_{x_1}c_{x_1}c_{x_2}\right. \\ &\quad \left. + d_{\text{ED}}IL\left(b_r c_{x_1}s_{x_2} + b_\vartheta s_{x_1}s_{x_2} - b_h c_{x_2}\right)\right]\Big/ Jc_{x_2} \\ \dot{x}_4 &= -(x_3 + \omega)^2 s_{x_2}c_{x_2} \\ &\quad - \left[3J\omega^2 s_{x_1}^2 s_{x_2}c_{x_2} + d_{\text{ED}}IL\left(b_r s_{x_1} - b_\vartheta c_{x_1}\right)\right]\Big/ J \end{aligned} \tag{31}$$

where $x_{1,4}$ are α, β, $\dot{\alpha}$, and $\dot{\beta}$, respectively, d_{ED} is the distance between the system's center of mass and the point where the ED force is applied, I is the current flowing into the tether, L is the length of the conductive segment of the tether, and b_r, b_ϑ, and b_h are the magnetic field components along the orbital axes. [They can be replaced by the SC TAM readings $\tilde{b}_1^{\text{sat}}$, $\tilde{b}_2^{\text{sat}}$ and $\tilde{b}_3^{\text{sat}}$, for what follows Eq. (16).]

Equation (31) represent a system of nonlinear differential equations that can be written in the form

$$\dot{\boldsymbol{x}} = \boldsymbol{f}\left(\boldsymbol{x}, J, d_{\text{med}}, i, L, \tilde{\boldsymbol{b}}^{\text{sat}}\right) + \xi \tag{32}$$

where ξ is a white zero-mean Gaussian process noise with power spectral density $\boldsymbol{Q}_c$, introduced here to account for all system model uncertainties.

The time propagation of the state estimate is performed using a standard fourth-order RK integrator. The nonlinear equations (32) are propagated between the sampling times t_k and t_{k+1} using a 0.005-s step.

The propagation of the error covariance matrix $\boldsymbol{P}_k$ is performed using the linearized dynamics state transition matrix, approximated as

$$\Phi_k \approx \boldsymbol{I} + \boldsymbol{F}_k\Delta t \tag{33}$$

where $\boldsymbol{I}$ is the 4×4 identity matrix, Δt is the sampling interval, and the Jacobian matrix $\boldsymbol{F}_k$ is computed as $\boldsymbol{F}_k = \partial \boldsymbol{f}/\partial x|_{x=\hat{x}}$.

Implementation Issues

The EKF is run in information form, in which the inverse of the error covariance matrix $\boldsymbol{P}_k$ is updated using the inverse of the predicted error covariance matrix $\boldsymbol{P}_k^-$. With this formulation, the filter is initialized with virtually no a priori information about the tether attitude/rates by setting the initial value of the inverse covariance (information) matrix to $(\boldsymbol{P}_0^-)^{-1} = \boldsymbol{I} \times 10^{-8}$ and the filter's initial estimate to $\hat{x}_0^- = [\boldsymbol{0}_{4\times 1}]$. This procedure results in a very high filter convergence rate, as has been verified in the numerical simulation study.

The optimal tuning of the filter is performed by adjusting the process noise covariance matrix $\boldsymbol{Q} \cong \boldsymbol{Q}_c \Delta t$, through a trial and error procedure. The final values used in the filter are $\boldsymbol{Q} = \boldsymbol{I} \times 10^{-12}$.

EKF Performance

The performance of the proposed estimation algorithm is evaluated through an extensive Monte Carlo simulation study, consisting of 300 runs, each lasting 1000 s. SC initial position along the 650-km altitude, 65-deg inclination circular orbit was randomly chosen in each simulation, and tether's initial attitude angles and rates were randomly sampled from uniform distributions, to bound the amplitude of the in-plane and out-of-plane libration angles to within 30 deg. In the simulations, the "real" tether attitude motion was numerically integrated taking into account the gravity gradient and ED torque in Euler's equations. The simulated TAM readings, sampled at a frequency of 1 Hz, were finally generated adding a zero-mean, white Gaussian noise, with a standard deviation of 50 nT, to the magnetic field vector computed, again using a 10th-order IGRF model.

The statistical results of the Monte Carlo simulation are summarized in Table 1; the ensemble-averaged mean errors are on the order of 10^{-4} deg and 10^{-5} deg/s, for the libration angles and rates, respectively, yielding a nearly unbiased filter. Moreover, the 1-σ estimation errors are small enough to allow a robust closed-loop control of the libration angles through the procedure described in the following section. Figures 7–10 show the performance of the filter in a typical run, in which the initial tether state is $\alpha = 2$ deg, $\beta = 5$ deg, and $\dot{\alpha} \equiv \dot{\beta} = 0$ deg/s.

Table 1 Statistical results of the Monte Carlo simulation study

Variable	Mean error	1-σ error
α, deg	2.17×10^{-4}	2.71×10^{-2}
β, deg	3.10×10^{-4}	4.72×10^{-2}
$\dot{\alpha}$, deg/s	3.44×10^{-5}	8.49×10^{-3}
$\dot{\beta}$, deg/s	3.19×10^{-5}	6.54×10^{-3}

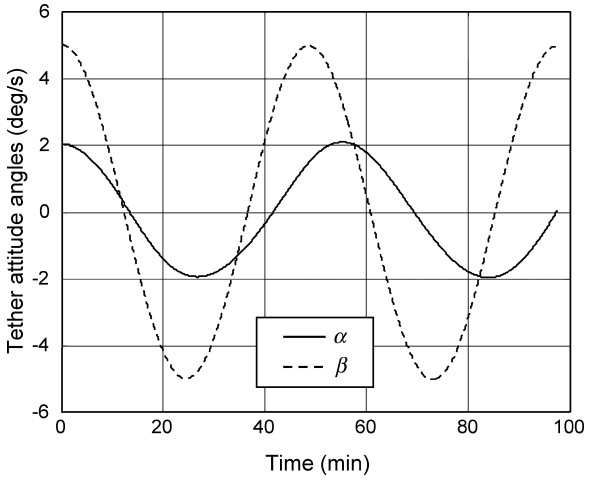

Fig. 7 Tether libration angles in typical run of Monte Carlo simulation.

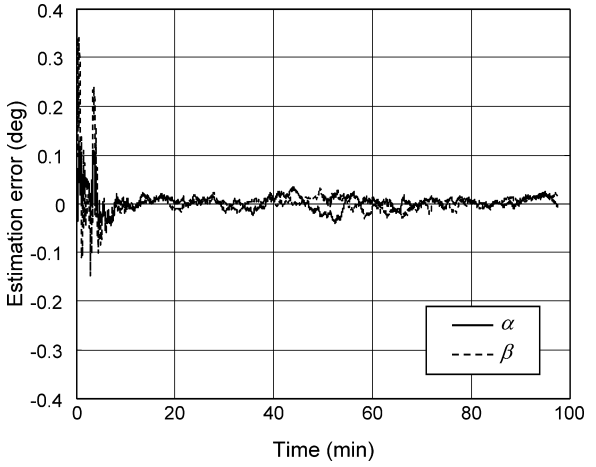

Fig. 8 Tether libration angles estimation errors in typical run of Monte Carlo simulation.

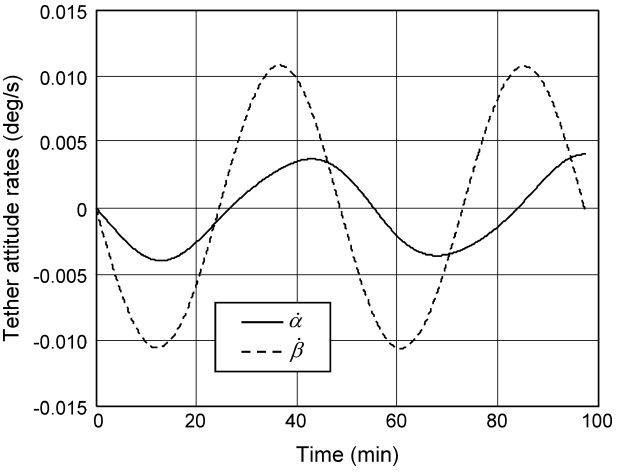

Fig. 9 Tether libration rates in typical run of Monte Carlo simulation.

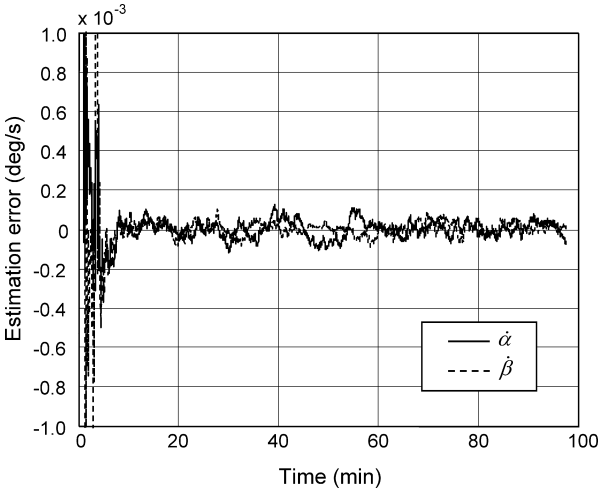

Fig. 10 Tether libration rates estimation errors in typical run of Monte Carlo simulation.

Actively Controlled Deorbiting Performance

When the described active current control is applied in the numerical simulations, making use of the EKF estimation of the variables α, β, $\dot{\alpha}$, and $\dot{\beta}$, results are similar to those obtained through the passive configuration (solid and dashed lines in Fig. 4). In particular,

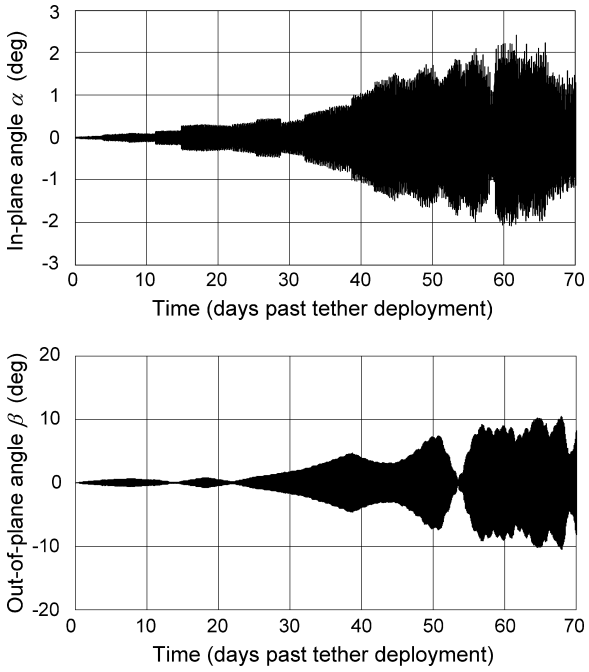

Fig. 11 Tether libration angles vs deorbiting time, controlled attitude.

when the thresholds 0.1 and 0 for the nondimensional Lyapunov function [Eq. (18″)] and the total ED power, respectively, are used, the total deorbiting time is increased by only a few days and the altitude-vs-time profile is changed only in the last part of the simulation, where the intermittent switching off of the tether current, slightly slows down the SC decay.

Figure 11 shows that when active tether current control is applied, the out-of-plane angle β is bounded to within 10 deg, leading to a very stable tether attitude motion. Direct comparison with Fig. 5 confirms that the tether control plays a role only in the last 10 days, when the increased tether current values are likely to destabilize its attitude motion.

VI. Conclusions

We have presented the design of a low-cost demonstration mission where a reduced-scale ED deorbiting system will be carried, deployed, and controlled by a microsatellite. Numerical simulations show that both the tether deployment phase and ED deorbiting of such a small system can be performed without active control because of the proposed configuration, obtained through a careful combination of bare and insulated tether segments. It has been shown that, even in the absence of active tether current control, the tether attitude is stable through the whole deorbiting phase, whereas when also active current control is applied, the tether libration angles are bounded to within 10 deg. This is obtained by means of a closed-loop control law making use of the in-plane and out-of-plane libration angles and rates, which are estimated through a newly developed EKF. We show that this microsystem is able to deorbit a LEO carrier SC in about two months, demonstrating salient features of tether technologies and associated ED effects.

Acknowledgments

P. Tortora acknowledges G. Piraccini, M. Tappi, and D. Bruzzi, from the ALMASat team, for producing the CAD drawings of the Micro-EDOARD payload and carrier spacecraft. This paper was presented as AAS Paper 04-168 at the 14th AAS/AIAA Space Flight Mechanics Conference, Maui, Hawaii, 8–12 February 2004.

References

[1]Forward, R. L., Hoyt, R. P., and Uphoff, C., "The Terminator Tether: A Near-Term Commercial Application of the NASA/MSFC ProSEDS Experiment," *Proceedings of the Tether Technology Interchange Meeting*, NASA CP-1998-206900, Jan. 1998, p. 109.

[2]Forward, R. L., Hoyt, R. P., and Uphoff, C., "Application of the Terminator Tether™ Electrodynamic Drag Technology to the Deorbit of Constellation Spacecraft," AIAA Paper 98-3491, July 1998.

[3]Iess, L., Bruno, C., Ulivieri, C., Vannaroni, G., Bertotti, B., Anselmo, L., Ponzi, U., Dobrowolny, M., De Venuto, F., Parisse, M., and Laneve, G., "Satellite Deorbiting by Means of Electrodynamic Tethers: General Concepts and Requirements," *Acta Astronautica*, Vol. 50, No. 7, 2002, pp. 399–406.

[4]Iess, L., Bruno, C., Ulivieri, C., and Vannaroni, G., "Satellite Deorbiting by Means of Electrodynamic Tethers: System Configuration and Performances," *Acta Astronautica*, Vol. 50, No. 7, 2002, pp. 407–416.

[5]Bruno, C., Bussolino, L., Iess, L., Licata, R., and Schirone, L., "EDOARD: A Tethered Device for Efficient Electrodynamic De-Orbiting of LEO Spacecraft," *Space Technologies and Applications International Forum* (STAIF 2001), Conf. Proceedings Vol. 552, American Inst. of Physics, Melville, NY, 2001, pp. 433–444.

[6]Bruno, C., Anselmo, L., Bussolino, L., Iess, L., Licata, R., Schirone, L., and Somenzi, L., "EDOARD: An Electrodynamic Tether Device for Efficient Spacecraft De-Orbiting," *Proceedings of the Third European Conference on Space Debris*, ESA, SP-473, Noordwijk, The Netherlands, 2001, pp. 707–712.

[7]Hoyt, R. P., and Forward, R. L., "Performance of the Terminator Tether for Autonomous Deorbit of LEO Spacecraft," AIAA Paper 99-2839, June 1999.

[8]Hoyt, R. P., and Forward, R. L., "The Terminator Tether: Autonomous Deorbit of LEO Spacecraft for Space Debris Mitigation," AIAA Paper 2000-0329, Jan. 2000.

[9]Vannaroni, G., Dobrowolny, M., and De Venuto, F., "Deorbiting with Electrodynamic Tethers: Comparison Between Different Tether Configurations," *Space Debris*, Vol. 1, No. 3, 2001, pp. 159–172.

[10]Heide, E. J., and van der Kruijff, M., "Tethers and Debris Mitigation," *Acta Astronautica*, Vol. 48, No. 5-12, 2001, pp. 503–516.

[11]Cosmo, M. L., and Lorenzini, E. C., *Tethers in Space Handbook*, 3rd ed., Smithsonian Astrophysical Observatory, Cambridge, MA, 1997, pp. 1–35.

[12]Dobrowolny, M. (ed.), "Special TSS-1 Issue," *Il Nuovo Cimento*, Vol. 17C, Jan.–Feb. 1994, pp. 1–141.

[13]Stone, N. H., and Bonifazi, C., "The TSS-1R Mission: Overview and Scientific Context," *Geophysical Research Letters*, Vol. 25, No. 4, 1998, pp. 409–412.

[14]McCoy, J. E., O'Neill, C., Stanley, J., Settecerri, T., Grossi, M. D., Estes, R. D., Dobrowolny, M., Vannaroni, G., Melchioni, E., Bonifazi, C., Cosmovici, C., Iess, L., Jost, R. J., Olsen, R. C., Ferguson, D. C., Tolbert, R., Rau, D., Katz, I., Lilley, J., Carroll, J. A., Taconi, G., Mina, L., and Goree, W., "Plasma Motor-Generator (PMG) Flight Experiment Results," *Proceedings of the 4th International Conference on Tethers in Space*, Science and Technology Corp., Hampton, VA, 1995, pp. 57–82.

[15]Carroll, J. A., "SEDS Deployer Design and Flight Performance," AIAA Paper 93-4764, Sept. 1993.

[16]Smith, H. F., "The First and Second Flights of the Small Expendable Deployer System," *Proceedings of the 4th International Conference on Tethers in Space*, Science and Technology Corp., Hampton, VA, 1995, pp. 43–55.

[17]Purdy, W., Coffey, S. L., Barnds, W. J., Kelm, B., and Davis, M., "TiPS: Results of a Tethered Satellite Experiment," *Advances in the Astronautical Sciences*, Vol. 97, Pt. 1, Aug. 1997, pp. 3–23.

[18]Johnson, L., and Balance, J., "Propulsive Small Expendable Deployer System (ProSEDS) Space Demonstration," *Proceedings of the Tether Technology Interchange Meeting*, NASA CP-1998-206900, Jan. 1998.

[19]Sanmartín, J. R., Martínez-Sánchez, M., and Ahedo, E., "Bare Wire Anodes for Electrodynamic Tethers," *Journal of Propulsion and Power*, Vol. 9, No. 3, 1993, pp. 353–360.

[20]Ahedo, E., and Sanmartín, J. R., "Analysis of Bare-Tether Systems for Deorbiting Low-Earth-Orbit Satellites," *Journal of Spacecraft and Rockets,* Vol. 39, No. 2, 2002, pp. 198–205.

[21]Carroll, J. A., and Oldson, J. C., "Tethers for Small Satellite Applications," *Proceedings of the AIAA/USU Small Satellite Conference*, Utah State Univ./AIAA, Logan, UT, 1995.

[22]Hoyt, R. P., Forward, R. L., Heinen, G., Slostad, J., and Minor, B., "The RETRIEVE Microsatellite Tether Deorbit Experiment," AIAA Paper 2002-3893, July 2002.

[23]Tortora, P., and Troiani, E., "The Microsatellite Research Program at Università di Bologna," *Acta Astronautica*, Vol. 56, No. 7, 2005, pp. 696–704.

[24]*Dnepr User's Guide*, No. 2, Nov. 2001, URL: http://www.kosmotras.ru [cited 1 Jan. 2005].

[25]Peláez, J., "Self Balanced Electrodynamic Tethers," AIAA Paper 2004-5309, Aug. 2004.

[26]Peláez, J., Sanjurjo, M., and Fontdecaba, J., "Satellite Deorbiting Using a Self Balanced Electrodynamic Tether," 55th International Astronautical Congress, Paper IAC-04-A.5.08, Oct. 2004.

[27]Peláez, J., and Sanjurjo, M., "Generator Regime of Self Balanced Electrodynamic Bare Tethers," 15th American Astronautical Society/AIAA Space Flight Mechanics Conf., AAS Paper 05-205, Jan. 2005.

[28]Peláez, J., Lorenzini, E. C., López-Rebollal, O., and Ruiz, M., "A New Kind of Dynamic Instability in Electrodynamic Tethers," *Journal of the Astronautical Sciences*, Vol. 48, No. 4, 2000, pp. 449–476.

[29]Dobrowolny, M., "Linear Stability of Electrodynamic Tethers," *Il Nuovo Cimento*, Vol. 25 C, No. 4, 2002, pp. 369–391.

[30]Dobrowolny, M., "Lateral Oscillations of an Electrodynamic Tether," *Journal of the Astronautical Sciences*, Vol. 50, No. 2, 2002, pp. 125–147.

[31]Chobotov, V. A., and Mains, D. L., "Tether Satellite System Collision Study," *Space Debris*, Vol. 1, No. 2, 2000, pp. 99–112.

[32]Patera, R. P., "Method for Calculating Collision Probability Between a Satellite and a Space Tether," *Journal of Guidance, Control, and Dynamics*, Vol. 25, No. 5, 2002, pp. 940–945.

[33]Hoyt, R. P., and Forward, R. L., "Failsafe Multistrand Tether SEDS Technology," *Proceedings of the 4th International Conference on Tethers in Space*, Science and Technology Corp., Hampton, VA, 1995, pp. 1151–1159.

[34]Forward, R. L., and Hoyt, R. P., "Failsafe Multiline Hoytether Lifetimes," AIAA Paper 95-2890, July 1995.

[35]Peláez, J., "On the Dynamics of the Deployment of a Tether from an Orbiter—I. Basic Equations," *Acta Astronautica*, Vol. 36, No. 2, 1995, pp. 113–122.

[36]Peláez, J., "On the Dynamics of the Deployment of a Tether from an Orbiter—II. Exponential Deployment," *Acta Astronautica*, Vol. 36, No. 6, 1995, pp. 313–335.

[37]"TMM and M Final Report," Alenia Spazio, Rept. TM-RP-AI-012, Turin, Italy, July 1994.

[38]Licata, R., and Gavira, J. M., "TMM&M Tether Deployment Mechanism Features and Test Results," *Proceedings of the 6th European Space Mechanisms and Tribology Symposium*, ESA, SP-374, Noordwijk, The Netherlands, 1995, pp. 119–136.

[39]Corsi, J., and Iess, L., "Stability and Control of Electrodynamic Tethers for Deorbiting Applications," *Acta Astronautica*, Vol. 48, No. 5-12, 2001, pp. 491–501.

[40]Denney, T. S., Jr., and Greene, M. E., "On State Estimation for an Orbiting Single Tether System," *IEEE Transactions on Aerospace and Electronic Systems*, Vol. 27, No. 4, 1991, pp. 689–695.

[41]Greene, M. E., and Denney, T. S., Jr., "Real-Time Estimator for Control of an Orbiting Single Tether System," *IEEE Transactions on Aerospace and Electronic Systems*, Vol. 27, No. 6, 1991, pp. 880–883.

N. Gatsonis
Associate Editor